Journal of Materials Chemistry A

ROYAL SOCIETY OF CHEMISTRY

PAPER

View Article Online
View Journal

Cite this: DOI: 10.1039/d5ta03402g

Titanium nitride prepared by the urea-glass synthesis gives an active electrocatalyst for the oxygen reduction reaction

Wanrui Xie, † Ryan D. Van Daele, † Allison Kaatz, Leo Ellenson, Fengrui Qu and Bart M. Bartlett *

Rock-salt-structured titanium nitride (TiN) has emerged as a leading earth-abundant electrocatalyst for the oxygen reduction reaction (ORR). We compare TiN prepared in three ways starting from urea: the urea–glass method, by a direct reaction between urea and titanium(IV) chloride, and through a discrete monomeric complex. In the urea-glass route, a new-found $[Ti_4(\mu\text{-}O)_6(OC(NH_2)_2)_{12}]^{4+}$ oxo-bridged titanium–urea precursor can be synthesized in a single-pot reaction at room temperature starting from titanium(IV) chloride, urea, and ethanol with a urea-to-titanium ratio of 6. Subsequent annealing of the polymeric gel that results at 750 °C in an N_2 atmosphere yields phase-pure, TiN particles on the 100 μm size scale. TiN can be deposited as an ink with PiperION®anion exchange dispersion onto a glassy carbon rotating disk electrode (RDE), and of the three synthesis methods, the urea-glass method gives the most active ORR catalyst. The onset potential for ORR activity is −131 mV *vs.* Hg/HgO, and Koutecký–Levich analysis of linear-sweep voltammetry recorded at varying rotation rates supports a two-electron reduction pathway to H_2O_2, with a rate constant of 0.0172 cm s^{-1}. The higher activity is ascribed to a more oxygen-rich surface—boh defect sites and active oxygen species—afforeded by the oxo-bridged precursor, corrorborated by X-ray photoelectron spectroscopy (XPS) analysis.

Received 29th April 2025
Accepted 5th December 2025

DOI: 10.1039/d5ta03402g

rsc.li/materials-a

Introduction

The concept of a green hydrogen economy has garnered significant attention due to concerns about the depletion of fossil fuel reserves and the environmental challenges stemming from their overconsumption.[1] In the transportation sector, fossil fuels still dominate as the primary energy source.[2] However, due to the accelerated depletion of fossil fuels, developing alternative sources for sustainable energy storage and conversion has gained much attention over the past quarter century. Alkaline anion-exchange membrane fuel cell (AEMFCs) and rechargeable metal-air batteries have emerged as promising technologies for clean energy storage and conversion. In these systems, the oxygen reduction reaction (ORR) at the cathode is a critical but challenging step, particularly due to the slow multi-electron transfer steps (especially *O–O bond breaking, *OOH, *OH intermediates).[3,4] To address this limitation, selecting an appropriate catalyst that offers optimal adsorption of oxygen intermediates and facilitates O–O bond cleavage is crucial for enhancing the rate.[5,6] Currently, platinum and iridium are effective catalysts, but their high cost and scarcity limit large-scale production. This situation underscores the urgent need to develop low-cost, high activity electrocatalysts.[7] There has been a lot of recent attention on transition-metal sulfides, borides, carbides, and nitrides. Among these classes of materials, the transition-metal nitrides (TMNs) stand out as having high conductivity, scalable syntheses, and sufficient stability with respect to corrosion,[8] due to their unique metallic electronic structure.[9]

In particular, rock-salt structured titanium nitride (TiN) is highly stable, less expensive than platinum, and exhibits good electrical conductivity as an electrode.[10–12] Accordingly, there are several examples of its use as an ORR electrocatalyst in AEMFCs.[13–15] It is notably more active than W_2N, NbN, and Ta_3N_5.[16,17] To date, the primary synthesis routes for TMNs include direct ammonolysis of precursors, solvothermal methods, impregnation adsorption methods, chemical vapor deposition, and carbonization of metal–organic framework materials.[18–20] These synthesis methods often require high temperatures (1000 °C) or high pressures (60 bar)[21] and flowing toxic ammonia, which complicates the procedures in a way that limits scaling the reactions.

An alternative approach for synthesizing TMNs is the urea-glass pathway, which uses metal chlorides and urea as the precursors. Several papers have discussed this method to synthesize various metal nitrides.[22–24] In general, the procedure is to dissolve the desired metal chloride salt in ethanol solvent and to add urea, which presumably forms a coordination complex that reacts further to form a glass (polymeric gel). The

Department of Chemistry, University of Michigan, USA. E-mail: bartmb@umich.edu
† W. X. and R. D. V. D. contributed equally to this work.

entire solution is then placed in a tube furnace under flowing nitrogen gas and heated to 750 °C, where urea decomposes to generate ammonia, water, and other products such as isocyanic acid (HNCO), biuret [$HN(CONH_2)_2$], cyanuric acid ($C_3H_3N_3O_3$), and ammelide ($C_3H_4N_4O_2$).[25,26] This approach was initially reported for synthesizing TiN, VN, NbN, GaN, Mo_2N, W_2N, CrN, and others,[27] and it has been expanded to include oxynitride materials as well.[28–30]

The glass decomposition proceeds through two potentially competing routes: one dominated by ammonia evolution, which ultimately favors metal nitride formation, and another that produces water, promoting the formation of metal hydroxides and, upon dehydration, metal oxides.[28] The predominance of either pathway is closely linked to the urea-to-metal chloride molar ratio (R). When the quantity of urea in the reactant mixture is insufficient, ammonia generation is limited, which suppresses the formation of pure TMNs. Conversely, an excess of urea enhances ammonia production, thereby increasing the likelihood of nitride formation. Using titanium nitride synthesis as an example, it has been observed that a glassy intermediate containing anatase and rutile TiO_2 first appears at approximately 400 °C, and upon heating to 600 °C, oxygen loss accompanied by metal reduction and nitridation is observed. Complete transformation from titania to titanium nitride typically occurs at around 800 °C.[30] However, insufficient nitridation time leads to incomplete conversion and the persistence of oxide impurities.[31] But TiN never forms directly,[32] which leads to a question of the structure and composition of any reaction intermediates. In the urea-glass synthesis of the main group nitride AlN, an easily isolable homoleptic octahedral complex between Al^{3+} and six urea molecules bound through their O-atoms forms.[33] Accordingly, the optimal urea-to-metal molar ratio is 6 : 1, and lower R ratios lead to persistent aluminum oxide impurities.[8,9] Although the structure of hexakis(urea) titanium(III) chloride complex is known,[34] only the bis(urea) titanium(IV) chloride complex has been identified. The increased electropositivity of Ti(IV) over Ti(III) results in preference for X-type chloride ligands over L-type urea ligands.[35]

A critical question for our study is: how does the urea content in the reactant mixture influence not only the phase purity, but also the surface composition that maximizes ORR activity? It is known for ZrN that some 15 equivalents of urea are needed to give phase pure material with excellent electrical conductivity and a sufficiently hydroxylated surface that facilitates ORR reaction kinetics.[36] We focus on TiN because there we have identified three ways to combine titanium(IV) chloride and urea to yield phase pure material: (1) urea-glass method in ethanol solvent under varying R ratios 2, 4, and 6; (2) a direct solventless reaction between liquid $TiCl_4$ and urea; (3) a molecular precursor method from a known reaction between $TiCl_4$ and two equivalents urea in an inert solvent (dichloromethane), which does not form a glass.[37] All methods form phase-pure TiN, and all reduce O_2 to H_2O_2, which is expected under basic conditions.[38] We compare the electrocatalytic activity in light of the surface functionality to identify the link between the oxygen content in the reactant mixture and the ORR activity. By establishing the connection between the precursor structure and composition, and the required urea our findings pave the way for scalable, predictable synthesis of a variety of TMNs that are active ORR electrocatalysts.

Experimental

Synthesis of TiN

Urea glass method. 3.51 mmol titanium tetrachloride (Sigma-Aldrich) was added to 2 mL ethanol (>99.5 vol%, Fisher) under an N_2 atmosphere. The reaction is exothermic, and after the solution returned to the room temperature, the desired amount of urea (Fisher Scientific) was added: 2, 4, or 6 equivalents based on the starting quantity of titanium. The mixture was stirred until dissolved, transferred to an aluminium crucible, and heated in flowing N_2 gas at 750 °C for 3 hours with a heating and cooling rate of 3 °C per min. When 2 equivalents of urea were added (7.02 mmol of urea) the isolated yield was 0.1236 g (56.9%). When 4 equivalents of urea were added the isolated yield was 0.2007 g (92.4%). When 6 equivalents or urea were added (21.06 mmol of urea), the isolated yield is 0.1957 g (90.1%).

Direct solventless reaction. 3.51 mmol titanium tetrachloride (Sigma-Aldrich) was mixed with the desired amount of urea (Fisher Scientific) under an N_2 atmosphere. The mixture was left in the dry N_2 box (Vacuum Atmospheres) overnight, and heated in flowing N_2 at 750 °C for 3 hours with a heating and cooling rate of 3 °C per min. The isolated yield was 0.0623 g (3.3%).

Molecular precursor method. In a dry N_2 box, 0.33 g urea (5.5 mmol) was placed in 50 mL methylene chloride and then 10.3620 g of $TiCl_4$ (54.78 mmol) was added. The reaction was stirred for 6 days at 800 rpm. The solid was rinsed 3 times with methylene chloride (Fisher) the isolated yield was 0.8068 g (94.7%). 0.7555 g of $TiCl_4(OC(NH_2)_2)_2$ was added to a crucible put into a quartz tube and transferred onto the tube furnace air free. The sample was annealed to 750 °C for 3 hours with a ramp and cool rate of 3 °C per min. The isolated yield is 0.1274 g (84.6% yield based on starting urea).

All products were stored under ambient conditions for further use. Details for the single crystal diffraction experiment and crystallographic data (Tables S1–S6) are presented in the SI.

Preparation of electrodes. All experiments were conducted at room temperature. Before the experiment, a 5 mm glassy carbon electrode (GCE, CH Instruments, Inc.) was polished using 0.3 μm and 0.05-μm aluminum oxide polishing slurry and washed with ethanol and Milli-Q water in an ultrasonic bath. The homogeneous inks for electrochemical measurements were prepared by adding a mixture of 8 mg of titanium nitride sample to a solution of 480 μL of 18.2 MΩ Milli-Q water, 480 μL of isopropanol (supplier), and 40 μL of PiperlON®anion exchange dispersion (Fuel Cell Earth, 5 wt%, aq.) and then sonicating for 30 min. Then 30 μL of the catalyst inks were coated onto the clean GCE.

Electrochemical reaction conditions. Rotating disk electrode (RDE) measurements were performed using an RRDE-3A (ALS Japan) connected to a CHI760E electrochemical workstation. The measurements employed a three-electrode setup, with Hg/HgO used as the reference electrode, a 3 mm GCE as the counter

electrode, and the working electrode described above. 25 mL of a 0.1 M KOH solution (pH 13) was used as the electrolyte for the electrochemical measurements. Before the RDE measurements, the electrolyte was saturated with O_2 gas for 20 minutes, and O_2 was continuously sparged into the electrolyte during the measurements.

Permanganate test of H_2O_2 in the electrolyte. A 5 mM $KMnO_4$ solution was prepared, and two sets of experiments were conducted. In the experimental setup, the electrolyte consisted of a mixture of 0.5 mL 2.0 M H_2SO_4 and 1 mL of 0.1 M KOH, collected after running of TiN over 8 hours at a fixed potential of −0.5 V *vs.* Hg/HgO and a rotation rate of 1600 rpm under O_2-saturated conditions. The control setup used a mixture of 0.5 mL 2.0 M H_2SO_4 and 1 mL of 0.1 M KOH solution without prior LSV operation. To each setup, 15 μL of the 5 mM $KMnO_4$ solution was added, and the resulting colour changes were recorded.[39]

Materials characterization. X-ray diffraction (XRD) analysis was performed using a Panalytical Empyrean diffractometer operating at 1.8 kW power (45 kV, 40 mA) with Cu Kα radiation ($\lambda = 1.5418$ Å). A zero-background holder made of single-crystal silicon was utilized for the measurements. The scan rate and step size were 0.07°/s and 0.033°, respectively. Scanning electron microscopy (SEM) was performed using a JEOL-7800FLV FE-SEM equipped with an energy-dispersive X-ray spectrometry (EDX) system. The EDX analysis was conducted with an Oxford XMaxN 80 mm^2 silicon-drift detector and processed using Oxford Aztec v3.3 software for data acquisition and analysis. Fourier transform infrared spectroscopy (FTIR) analysis was collected with Thermo-Nicolet IS-50 with 0.1 cm^{-1} resolution. X-ray photoelectron spectroscopy (XPS) was collected on a Kratos Axis Supra+ using Al Kα (1486.6 eV) radiation with 0.25 eV line resolution and 0.44 eV instrument resolution. The spectra were corrected for charging by referencing the C(1s) peak to 284.8 eV. Peak fitting and analysis were carried out using Casa XPS software.

Results and discussion

Synthesis insights, structural intermediates, and morphology of titanium nitride

Starting with an exploration of the traditional urea-glass route, we carried out the reaction using urea-to-metal chloride molar ratios $R = 2$, 4, and 6. The XRD patterns (Fig. 1a) show that when $R < 6$, both anatase and rutile phases of TiO_2 are present, indicating incomplete nitridation. In contrast, when $R = 6$, phase-pure TiN results. In this $R = 6$ case, we isolate a molecular complex as an intermediate, $[Ti_4(\mu\text{-}O)_6(OC(NH_2)_2)_{12}]^{4+}$, whose single-crystal structure is illustrated (Fig. 1b). Details for the crystal growth experiment, data collection, and the relevant tables are provided in the electronic supplementary information. In this complex, each Ti^{4+} adopts a distorted octahedral coordination environment comprising three urea ligands and three bridging oxygen atoms in a facial arrangement. The bridging oxos likely stem from residual water in the ethanol solvent. This mixed coordination stabilizes the structure by balancing charge distribution and steric effects. Unlike Al^{3+},

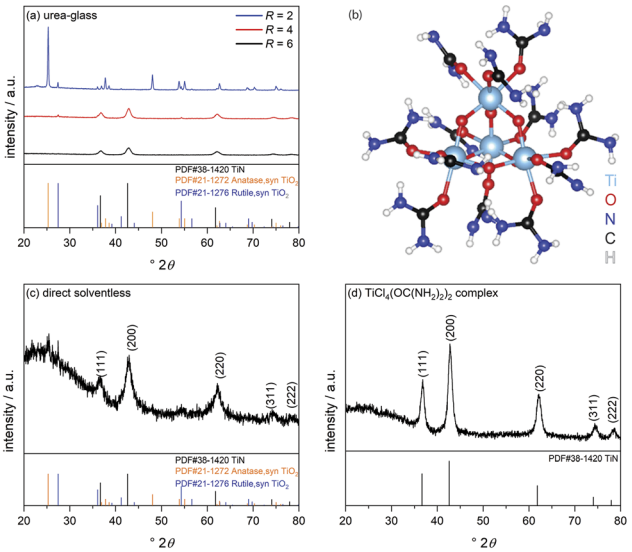

Fig. 1 (a) Powder XRD patterns of TiN prepared by the urea-glass method at using $R = 2$, 4, and 6; (b) structure of the urea-glass precursor cation $[Ti_4(\mu\text{-}O)_6(OC(NH_2)_2)_{12}]^{4+}$ from single-crystal XRD; (c) powder XRD of TiN obtained by the direct solventless route; (d) powder XRD of TiN obtained from the discrete molecular precursor $TiCl_4(OC(NH_2)_2)_2$.

which forms a homoleptic urea complex, Ti^{4+} is strongly oxophilic and readily undergoes hydrolysis when water is present; subsequent condensation leads to the oxo-bridged Ti–O–Ti network.[40]

By integrating literature on urea thermal decomposition and the transformation of TiO_2 to TiN under ammonlysis by flowing ammonia, we hypothesize a stepwise process in which the complex decomposes to yield both NH_3 and H_2O; Ti^{4+} undergoes hydrolysis with the generated H_2O to afford titanium oxide; and nitridation by NH_3 then replaces oxygen in the oxide to form TiN. This model suggests that ethanol, used to create the urea-glass, may not be required to generate TiN. Accordingly, we carried out a direct solventless reaction in which we physically mixed liquid $TiCl_4$ with solid urea at $R = 6$ overnight in a dry nitrogen glovebox, subjected the mixture to tube-furnace treatment, and characterized the product by XRD (Fig. 1c). The data indicate that TiN with small quantities of anatase and rutile TiO_2 can be produced without first forming a homogeneous ethanol solution.

We posit that oxide-rich precursors necessitate more extensive nitridation—*i.e.*, greater consumption of urea—to obtain phase-pure titanium nitride. Accordingly, we turned to a known reaction to generate a molecular complex of titanium, $TiCl_4(OC(NH_2)_2)_2$, reported by Rivest in 1962,[35] of urea in a non-reactive solvent, dichloromethane. This synthesis specifically minimizes O-atom incorporation in the precursor. We performed ATR-IR characterization of the complex. (Fig. S1), where we observe clear shifts in the N–H and C–H stretching bands of urea upon complex formation. Subjecting this isolated molecular complex to the same tube-furnace treatment yields phase-pure TiN in the absence of any oxide impurity (Fig. 1d). These

results demonstrate that the extent of nitridation depends primarily on the precursor's structure: the greater the oxide content in the precursor, the more nitrogen from urea is needed to complete the TiO_2 to TiN chemical transformation.

SEM images for TiN prepared by three routes are shown in Fig. 2. The $TiCl_4(OC(NH_2)_2)_2$ precursor route and the direct solventless route yield smaller particles than the urea-glass method. Urea-glass TiN consists of plate-like particles on the ~100 μm scale, whereas the direct solventless route forms aggregates of similar lateral dimensions. Using $TiCl_4(OC(NH_2)_2)_2$ as the starting complex reduces particle aggregation. More images are provided in Fig. S2. EDX mapping (Fig. S3) indicates that for the sample derived from urea-glass synthesis, the average nitrogen atomic percentage is ~29% on the plate surfaces and ~47% on the smaller particles. For the direct solventless sample, the average nitrogen and oxygen atomic percentages are 27% and 73%, respectively. For TiN prepared from the complex, $TiCl_4(OC(NH_2)_2)_2$, the averages are 47% N and 53% O. Overall, the greater aggregation/larger particle size correlates with a higher oxygen content, whereas smaller particles show a higher nitrogen content.

As outlined in the introduction, previous research has shown that during urea–glass synthesis of transition-metal nitrides (TMNs), the initial step is formation of the corresponding metal oxide. Subsequently, nitrogen produced by urea decomposition gradually substitutes for oxygen in the oxide, leading to nitride formation.[31,32] Taken together, the three TiN syntheses show that minimizing oxygen in the precursor or during processing reduces the amount of oxide observed in the product. These observations align with our hypothesis that greater oxide content in the precursor necessitates increased urea consumption (the nitriding source) to achieve complete conversion to TiN. Additionally, to confirm that urea is the only nitride source in our synthesis, we prepared TiN at $R = 6$ under both N_2 and Ar atmospheres; the XRD patterns (Fig. S4) showed no differences, indicating that these gases are inert in this reaction. Furthermore, we isolated the powder obtained from the single-crystal growth experiment in the urea-glass synthesis, and subjected it to heat treatment in flowing nitrogen at 750 °C for 3 hours with a heating and cooling rate of 3 °C per minute. The XRD pattern (Fig. S5) confirms that this material yields phase-pure TiN.

Oxygen reduction reaction (ORR) activity of TiN prepared by the three methods

To further investigate the oxygen reduction reaction (ORR) activity and elucidate the reaction kinetics of TiN catalysts prepared by three different methods, LSV traces of three different TiN catalyst inks were recorded. Polarization curves were obtained by scanning the potential from 0 to −0.7 V *vs.* Hg/HgO at a scan rate of 100 mV s^{-1} in 0.1 M KOH, with rotation rates ranging from 1225 to 2500 rpm under O_2-saturated conditions (Fig. 3a). For comparison, the experiment was also performed using a blank glassy carbon electrode (GCE). As expected, all three TiN catalysts exhibited higher current densities and more positive onset potentials compared to the control GCE. Furthermore, the limiting current density increased with higher rotation rates for all three TiN catalysts, consistent with typical ORR behavior. Interestingly, despite the smaller particle sizes and lower surface oxygen content of the TiN catalysts prepared by the direct solventless reation and the $TiCl_4(OC(NH_2)_2)_2$ complex, their ORR activity is inferior to that of TiN prepared by the urea-glass method. The onset potential of the urea-glass TiN was −0.131 V *vs.* Hg/HgO, accompanied by a higher current density compared to the other two. TiN prepared by the other synthesis methods exhibit onset potentials of approximately −0.193 V *vs.* Hg/HgO. These results suggest that a higher oxygen content on the TiN surface enhances ORR catalytic activity, which is consistent with the findings of Zhu *et al.*, who demonstrated that introducing oxygen into TiN generates an oxygen-defect-rich TiO_xN_Y shell, that promotes ORR by creating abundant, defect-rich interfacial sites.[41]

We also conducted RDE tests on TiN prepared by the urea-glass method with lower R values, 2 and 4 (Fig. S6). Interestingly, the $R = 4$ sample exhibits the highest ORR activity, even though it contains some remaining TiO_2. This result suggests that the presence of an oxide may facilitate the ORR reaction. We do, however, observe a limit to this beneficial activity; the $R = 2$ sample shows a slightly more negative onset potential than the original $R = 6$ version. The enhanced ORR activity observed in the mixed-phase Ti samples agrees with the results of Zeng *et al.*,[42] who found that introducing oxide species on nitride surfaces can facilitate charge transfer and stabilize oxygen intermediates, leading to improved electrocatalytic activity.

To evaluate the practical applicability of the TiN electrodes in fuel cells, stability is a critical factor. Fig. 3b presents the

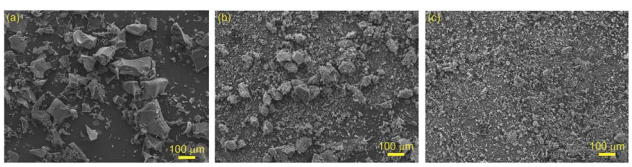

Fig. 2 SEM images of TiN synthesized by (a) urea-glass synthesis; (b) the direct solventless route; and (c) from $TiCl_4(OC(NH_2)_2)_2$. Each image is recorded using 20.0 keV electrons, a 10-mm working distance, and 100× magnification.

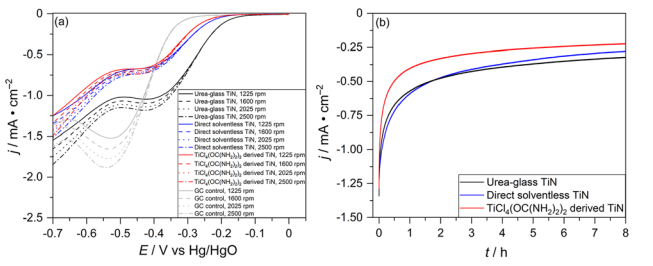

Fig. 3 (a) LSV traces of the ORR on TiN prepared by the three different methods (urea-glass, black; direct-solventless, blue; and from $TiCl_4(OC(NH_2)_2)_2$, red) and the bare GCE (gray) in O_2 saturated 0.1 M KOH solution at various rotation rates using an RDE set-up; the scan rate is 100 mV s^{-1}; (b) CPC traces of the ORR on TiN electrodes prepared by the three different methods (same color scheme), measured over 8 hours at a fixed potential of −0.5 V *vs.* Hg/HgO and a rotation rate of 1600 rpm.

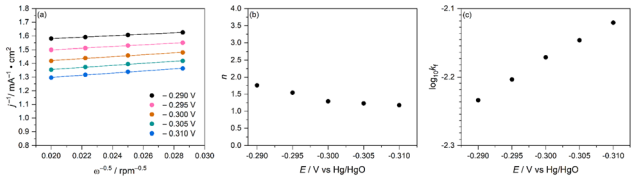

Fig. 4 The corresponding kinetic details derived from the previous figure for urea-glass prepared TiN (a) the Koutecký–Levich plot; (b) corresponding electron transfer numbers; and (c) the forward constant rate as a function of applied potential.

controlled potential chronoamperometry (CPC) data for the three types of TiN during an 8 hour ORR experiment. A consistent steady-state cathodic current density between 0.25 and 0.38 mA cm^{-2} is observed maintained throughout the duration without any signs of decline, demonstrating the catalyst's high stability. The corresponding Koutecký–Levich plot for the $R = 6$ urea-glass TiN RDE data is shown in Fig. 4a. The analyses for TiN prepared by the other two methods are provided in Fig. S7 and S8. TiN synthesized by all three different methods exhibits good linearity and parallel trends over the same potential range, confirming a consistent electron-transfer number per O_2 molecule and a first-order dependence of ORR kinetics on O_2 concentration.[43,44] The electron-transfer number (n) for the ORR on TiN was determined from the slope, using the Koutecký–Levich equation:[45] slope $= (0.62nFAC_0{}^*D_0{}^{2/3}\nu^{-1/6})^{-1}$, where n is the number of electrons transferred, A is the electrode area (0.2846 cm^2), F is the Faraday constant (96 485C mol^{-1}), C_0 is the bulk concentration of O_2 (1.2×10^{-3} M), D_0 is the diffusion coefficient of O_2 in 0.1 M KOH electrolyte (1.9×10^{-5} cm^2 s^{-1}, and ν is the kinematic viscosity of the electrolyte (1.09×10^{-2} cm^2 s^{-1}). Based on this analysis, the calculated number of electrons transferred during the ORR on traditional urea-glass synthesized TiN is 1.7 (Fig. 4b) which corresponds closely to the classical two-electron reduction pathway of O_2 to H_2O_2 ($O_2 + 2H_2O + 2e^- + \rightarrow H_2O_2 + 2OH^-$).[32] Additionally, the y-intercept of the Koutecký–Levich plot corresponds to the kinetic current at different potentials. Using the equation $i_k = FAk_f(E)C_0$, the forward rate constant (k_f) (Fig. 4c) for the ORR on traditional urea glass synthesized TiN is determined to be approximately 1.72×10^{-2} cm s^{-1} within the studied potential window;[25] this experiment was conducted in triplicate (Fig. S9 and Table S7). This rate constant is comparable to that observed on a bare GCE in a similar potential range (9.5×10^{-3} cm s^{-1} at −0.26 V *vs.* Hg/HgO in 0.1 M KOH), indicating competitive ORR kinetics for the urea-glass- synthesized TiN.[46] In contrast, the TiN prepared from either the direct solventless or from the $TiCl_4(OC(NH_2)_2)_2$ complex displayed lower electron-transfer numbers during the ORR, indicating reduced activity. Taken together, the LSV and Koutecký–Levich analyses consistently demonstrate that a higher surface oxygen content correlates with enhanced ORR activity in TiN catalysts.

Although the electron-transfer numbers for the ORR carried on TiN derived from the direct solventless method and from the $TiCl_4(OC(NH_2)_2)_2$ complex is marginally less than 2, we assume a two-electron ORR mechanism leading to hydrogen peroxide. To confirm that H_2O_2 is indeed the product for the three TiN variants, we conducted a qualitative test using potassium permanganate as an indicator.[47] As shown in Fig. S10, for the three types of TiN, following an 8-hour CPC experiment the intense violet ligand-to-metal charge-transfer (LMCT) band of permanganate vanishes immediately upon addition to the electrolyte solution, which is consistent with the expected reaction: $5H_2O_2 + 2MnO_4^-$ (violet) $+ 6H^+ \rightleftharpoons 8H_2O + 5O_2 + 2Mn^{2+}$(colorless)

Monitoring changes in electrode composition by XRD, SEM, and XPS analysis

To evaluate changes in the catalyst surface composition after the ORR, we employed a suite of characterization techniques. XRD shows that no new phases emerge after the ORR; only rock-salt structured TiN is present (Fig. S11). Moreover, SEM imaging shows no morphological changes to the TiN particles (Fig. S12); plate-like particles on the 10 μm scale are still observable.

Despite seeing no changes in the bulk composition or morphology, X-ray photoelectron spectroscopy (XPS) does show that the electrocatalyst surface changes because of carrying out the ORR. Fig. 5 shows the O(1s) spectra collected pre- and post-ORR, with the binding energies and relative areas of each component provided in Table 1. All three preparation methods show a broad O(1s) feature that tails to higher binding energies and can be fit to two peaks. In particular, the high-binding-energy component (blue peak in Fig. 5) can be associated with surface hydroxide species; increases in this hydroxide environment correlate with enhanced ORR activity. The major component (brown peak in Fig. 5) is consistent with an amorphous

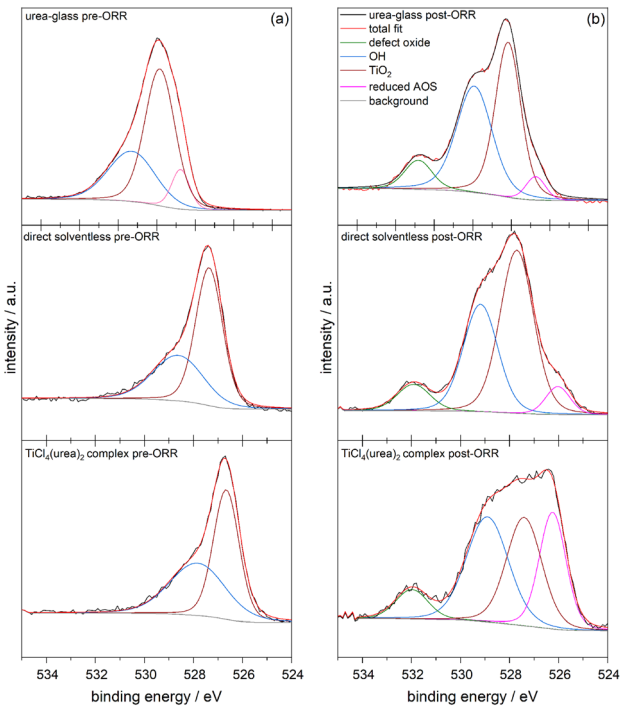

Fig. 5 XPS O(1s) analysis of urea-glass synthesized TiN, direct solventless reaction TiN, and $TiCl_4(urea)_2$ TiN (a) before the ORR and (b) after the ORR.

Table 1 O(1s) XPS data

Preparation method	B.E./eV pre-ORR	Area pre-ORR	B.E./eV post-ORR	Area post-ORR
Urea–glass				
Defect oxide	—	—	532.8	0.090
OH	531.3	0.328	529.9	0.419
TiO_2	529.8	0.572	528.2	0.442
Reduced AOS	528.8	0.100	526.0	0.049
Direct solventless				
Defect oxide	—	—	531.9	0.081
OH	528.6	0.381	529.2	0.345
TiO_2	527.4	0.619	527.7	0.511
Reduced AOS	—	—	526.0	0.063
$TiCl_4(OC(NH_2)_2)_2$complex				
Defect oxide	—	—	532.0	0.054
OH	527.8	0.467	528.2	0.253
TiO_2	526.7	0.533	526.6	0.406
Reduced AOS	—	—	526.0	0.287

surface TiO_2 layer. Notably, there is an additional peak in the sample prepared by the urea-glass synthesis at notably lower binding energy (pink peak in Fig. 5). This additional O(1s) component observed prior to the ORR likely represents reduced active oxygen species (AOS) on the surface that arises during the synthesis from the oxygen-rich precursor complex. This pre-existing AOS could facilitate the rapid reaction of oxygenated intermediates during ORR, which has been observed in MnN,[48] and helps explain why the urea-glass sample exhibits the highest ORR catalytic activity among the three preparation methods.

After the ORR, comparable low binding-energy oxygen species have been observed across all samples, which could be attributed to oxygen substituting into nitrogen sites within the TiN lattice, resembling Ti^{3+}–O or Ti_2O_3-like environments for the AOS. Notable is that as the peak area for this feature increases, the ORR activity decreases, hinting that having surface AOS inhibits the ORR. Both the solventless and $TiCl_4$(-urea)$_2$ samples initially contain a substantial amount of this species. We also note that after the ORR, all three preparation methods show the emergence of a higher binding-energy feature at ~532 eV, corresponding to a defect oxide species,[49,50] which could include under-coordinated oxygen and other non-lattice oxygen environments that can arise from surface-adsorbed ORR intermediates.[30] The urea-glass synthesis shows the highest ratio of defect oxide to AOS, which could explain the higher ORR activity if O_2 binds to the defect sites and requires the AOS to be released as H_2O_2 product forms.

The Ti(2p) XPS data (Fig. S13) for the three TiN samples further clarify the changes in surface oxidation states before and after ORR. Although Ti(2p) spectra are difficult to fit due to the presence of shake-up features and plasmons—and over-fitting can therefore be misleading—we chose to emphasize the raw spectra and focus primarily on the most intense Ti($2p_{3/2}$) peak, the oxide-like feature.[51] For the urea-glass TiN sample, prior to ORR the oxide-like peak in the envelope appears at 458.1 eV, and after ORR the high-binding-energy oxide portion decreases noticeably. This behavior is consistent with literature reports showing that when oxygen replaces nitrogen in titanium nitride, the effective charge on Ti decreases; consequently, the Ti(2p) binding energy shifts to lower values because Ti becomes more metallic (*i.e.*, less positively charged).[52] In Kroger Vink notation: $Ti_{Ti}N_N + O_s \rightarrow Ti'_{Ti}O_NN_i$ where O_s is an O-atom introduced from the surface and N_i is an interstitial (or other non-lattice) nitrogen. A similar trend is observed for the other two samples. For the direct-solventless sample, the Ti($2p_{3/2}$) oxide-like feature decreases in binding energy after ORR, shifting from 456.2 eV to 454.5 eV. For the $TiCl_4$(urea)$_2$-derived sample, this feature decreases, from 455.2 eV to 454.8 eV, indicating that more oxygen is incorporated after ORR.

The N(1s) spectra (Fig. S14) also confirm surface oxidation during ORR. The Ti–N peak in the envelope weakens after ORR across the samples, consistent with the classic TiN oxidation behavior described by Saha and Tompkins, where nitrogen loss leads to a reduced nitride contribution in N(1s).[53] A slight shift of the Ti–N peak toward lower binding energy is also observed, aligning with the expected perturbation of the Ti–N bonding environment. Among the three materials, the urea-glass TiN shows the smallest change in its N(1s) envelope, retaining a clear Ti–N peak with only modest attenuation. The $TiCl_4$(-urea)$_2$-derived sample exhibits a more noticeably weakened and broadened envelope, whereas the direct-solventless TiN shows nearly complete loss of the Ti–N feature. Since nitrogen retention is closely associated with preserving conductive TiN character, the well-maintained N(1s) signature in the urea-glass TiN provides a strong chemical basis for its superior ORR performance.

Conclusions

This study demonstrates three different synthesis methods for preparing titanium nitride (TiN): a traditional urea-glass starting from $TiCl_4$ and urea in ethanol, a direct solventless reaction between the $TiCl_4$ and urea precursors and heating an isolable

$TiCl_4(OC(NH_2)_2)_2$ complex. Combining the electrocatalytic activity with the surface composition by XPS, we note that in all cases, the electrode surface changes during the ORR to yield both defect oxides and residual active oxygen species. We find that the urea-glass synthesis generates an oxygen-rich intermediate, a polynuclear oxo-bridged Ti–urea complex, $[Ti_4(\mu\text{-}O)_6(OC(NH_2)_2)_{12}]^{4+}$ as verified by single-crystal X-ray diffraction. TiN synthesized by this urea-glass method exhibits the lowest overpotential for the ORR through the right balance of defect oxide and reduced AOS on the surface. Future work will focus on synthesizing other transition metal nitrides using the urea glass method with control of oxygen stoichiometry, particularly in the initial glass-forming step.

Author contributions

W. X. and R. D. V. D. contributed equally to this work. W. X. contributed through substantial contributions to the design of the work investigation, formal analysis, visualization of the data through graphics (XRD, LSV, SEM, XPS), and writing. R. D. V. D. contributed substantial contributions to the design of the work, investigation, formal analysis, visualization of the data through graphics and writing (TiN synthesis and SEM-EDS). A. K. contributed through investigation (TiN synthesis). L. E. contributed through investigation (LSV). F. Q. collected the single crystal structure. B. M. B. contributed through funding acquisition, supervision, and writing – review & editing.

Conflicts of interest

There are no conflicts to declare.

Data availability

The data supporting this article have been included as part of the supplementary information (SI). Supplementary information: experimental details for single crystal growth, data collection, and structure determination; crystallographic metrics and parameters, ATR-IR characterization, SEM images, EDX data, XRD patterns, additional LSV traces and electrochemical kinetics, photographs of the permanganate test, and additional XPS spectra. See DOI: https://doi.org/10.1039/d5ta03402g.

CCDC 2447455 contains the supplementary crystallographic data for this paper.[54]

Acknowledgements

This research was supported by a grant from the U.S. Department of Energy, Basic Energy Sciences, Catalysis Science Program, under Award No. DE-SC0006587. The authors acknowledge the financial support of the University of Michigan College of Engineering and NSF grant #DMR-0420785 (Kratos Axis Ultra XPS), and technical support from the Michigan Center for Materials Characterization. A. K. thanks the Arnold and Mabel Beckman Foundation for scholarship support. R. D. V. D. acknowledges funding support from the Chemistry President's Challenge Fellowship at the University of Michigan.

Notes and references

1 D. Y. C. Leung, X. Fu, C. Wang, M. Ni, M. K. H. Leung, X. Wang and X. Fu, *ChemSusChem*, 2010, **3**, 681–694.
2 F. Jaouen, E. Proietti, M. Lefevre, R. Chenniz, J. P. Dodelet, G. Wu, H. T. Chung, C. M. Johnston and P. Zelenay, *Energy Environ. Sci.*, 2011, **4**, 114–130.
3 H. A. Firouzjaie and W. E. Mustain, *ACS Catal.*, 2019, **10**, 225–234.
4 A. FUJISHIMA and K. HONDA, *Nature*, 1972, **238**, 37–38.
5 K. R. Yoon, C.-K. Hwang, S.-H. Kim, J.-W. Jung, J. E. Chae, J. Kim, K. A. Lee, A. Lim, S.-H. Cho, J. P. Singh, J. M. Kim, K. Shin, B. M. Moon, H. S. Park, H.-J. Kim, K. H. Chae, H. C. Ham, I.-D. Kim and J. Y. Kim, *ACS Nano*, 2021, **15**, 11218–11230.
6 K. Song, Y. Feng, W. Zhang and W. Zheng, *J. Energy Chem.*, 2022, **67**, 391–422.
7 B. Guo, J. Sun, X. Hu, Y. Wang, Y. Sun, R. Hu, L. Yu, H. Zhao and J. Zhu, *ACS Appl. Nano Mater.*, 2019, **2**, 40–47.
8 K. Kawashima, R. A. Marquez, L. A. Simth, R. R. Vaidyula, O. A. C. Jaim, Z. Q. Wang, Y. J. Son, C. L. Cao and C. B. Mullins, *Chem. Rev.*, 2023, **123**, 12795–13208.
9 H. Yang, C. Weng, H. Wang and Z. Yuan, *Coord. Chem. Rev.*, 2023, **496**, 215410.
10 B. Avasarala and P. Haldar, *Electrochim. Acta*, 2010, **55**, 9024–9034.
11 J. Theerthagiri, G. Durai, K. Karuppasamy, P. Arunachalam, V. Elakkiya, P. Kuppusami, T. Maiyalagan, H. S. Kim and J. of, *Ind. Eng. Chem.*, 2018, **67**, 12–27.
12 Z. Jin, P. Lin and D. Xiao, *Sci. Rep.*, 2014, **4**, 6712.
13 R. Onishi, M. Katayama, D. Cha and K. Takanabe, *J. Electrochem. Soc.*, 2013, **160**, 501–506.
14 Y. Wang, R. Ohnishi, E. Yoo, P. He, J. Kubota, K. Domen and H. hou, *J. Mater. Chem.*, 2012, **22**, 15549–15555.
15 H. Zhang, J. Liu, X. Li, X. Duan, M. Yuan, F. Cao, K. Sun, Y. Zhang, Y. Wang, Z. Gu, J. Li and J. Liu, *RSC Adv.*, 2022, **12**, 25035–25040.
16 D. H. Youn, G. Bae, S. Han, J. Y. Kim, H. Park, S. H. Choi and J. S. Lee, *J. Mater. Chem. A*, 2013, **1**, 8007–8015.
17 D. Zhang, D. Zhang, Z. Xie, B. Xu, M. Hou, Y. Lei, T. Watanabe, B. Yang and F. Liang, *Materials*, 2023, **16**, 7469.
18 Q. Luo, C. Lu, L. Liu and M. Zhu, *Green Energy Environ.*, 2023, **8**, 406–437.
19 R. S. Ningthoujam and N. S. Gajbhiye, *Prog. Mater. Sci.*, 2015, **70**, 50–154.
20 Z. Yang, H. Xu, T. Shuai, Q. Zhan, Z. Zhang, K. Huang, C. Dai and G. Li, *Nanoscale*, 2023, **15**, 11777.
21 S. Carole, N. Frety, S. Etienne-Calas, C. Merlet and R. M. Marin-Ayral, *Mater. Sci. Eng., A*, 2006, **419**, 365–371.
22 J. J. Brancho, A. D. Proctor, S. Panuganti and B. M. Bartlett, *Dalton Trans.*, 2017, **46**, 12081–12087.
23 X. Hu, W. Tian, Z. Wu, X. Li, Y. Li and H. Wang, *J. Colloid Interface Sci.*, 2024, **672**, 610–617.

24 S. C. H. Bragulla, A. R. V. Seggern, J. Lorenz, C. Harms, M. Wark and K. A. Friedrich, *ChemCatChem*, 2024, **16**, e202400613.
25 S. Tischer, M. Bornhorst, J. Amsler, G. Schoch and O. Deutschmann, *Phys. Chem. Chem. Phys.*, 2019, **21**, 16785–16797.
26 P. M. Schaber, J. Colson, S. Higgins, D. Thielen, B. Anspach and J. Brauer, *Thermochim. Acta*, 2004, **424**, 131–142.
27 C. Giordano, C. Erpen, W. Yao, B. Milke and M. Antonietti, *Chem. Mater.*, 2009, **21**, 5136–5144.
28 J. J. Brancho, A. D. Proctor, S. Panuganti and B. M. Bartlett, *Dalton Trans.*, 2017, **46**, 12081–12087.
29 X. Hu, W. Tian, Z. Wu, X. Li, Y. Li and H. Wang, *J. Colloid Interface Sci.*, 2024, **672**, 610–617.
30 S. C. H. Bragulla, A. R. V. Seggern, J. Lorenz, C. Harms, M. Wark and K. A. Friedrich, *ChemCatChem*, 2024, **16**, e202400613.
31 M. Afkari, P. Liu, V. Briois, J. Claverie and A. Wustrow, *Inorg. Chem.*, 2025, **64**, 14853–14863.
32 H. Zhang and J. F. Banfield, *Chem. Rev.*, 2014, **114**, 9613–9644.
33 H. Chaurasia, S. K. Tripathi, K. Bilgaiyan, A. Pandey, K. Mukhopadhyay, K. Agarwal and N. E. Prasad, *New J. Chem.*, 2019, **43**, 1900–1909.
34 J. Li, X. Yang and T. Ishigaki, *J. Phys. Chem. B*, 2006, **110**, 14611–14618.
35 R. Rivest, *Can. J. Chem.*, 1962, **40**, 2234–2242.
36 S. C. Bragulla, A. R. van Seggern, J. Lorenz, C. Harms, M. Wark and K. A. Friedrich, *ChemCatChem*, 2024, **16**, e202400613.
37 R. Rivest, *Can. J. Chem.*, 1962, **40**, 2234–2242.
38 S. Li, L. Shi, Y. Guo, J. Wang, D. Liu and S. Zhao, *Chem. Sci.*, 2024, **15**, 11188–11228.
39 A. Byeon, W. Yun, J. Kim and J. W. Lee, *ChemElectroChem*, 2023, **10**, e202300234.
40 U. Schubert and B. Stoger, *Chem. Eur. J.*, 2024, 30.
41 X. Zhu, Z. Zhao, J. Tang, X. Peng, H. Um, X. Li, Q. Xiao and W. Luo, *Fundam Res.*, 2023, **5**, 1134–1143.
42 R. Zeng, H. Li, Z. Shi, L. Xu, J. Meng, W. Xu, H. Wang, Q. Li, C. J. Pollock, T. Lian, M. Mavrikakis, D. A. Muller and H. D. Abruna, *Nat. Mater.*, 2024, **23**, 1695–1703.
43 A. J. Bard and L. R. Faulkner, *Electrochemical Methods*, Jogn Wiley & Son, 1944.
44 Y. Dong, Y. Wu, M. Liu and J. Li, *ChemSusChem*, 2013, **6**, 2016–2021.
45 J. Xu, G. Dong, C. Jin, M. Huang and L. Guan, *ChemSusChem*, 2013, **6**, 493–499.
46 M. Siddika, N. Hosen, R. H. Althomali, J. Y. Al-Humaidi, M. M. Rahman and M. A. Hasnat, *Catalysis*, 2024, **14**, 164/1–11.
47 C. Kim, S. O. Park, S. K. Kwak, Z. Xia, G. Kim and L. Dai, *Nat. Commun.*, 2023, **14**, 5822.
48 R. Zeng, H. Li, Z. Shi, L. Xu, J. Meng, W. Xu, H. Wang, Q. Li, C. J. Pollock, T. Lian, M. Mavrikakis, D. A. Muller and H. D. Abruna, *Nat. Mater.*, 2024, **23**, 1695–1703.
49 G. Beamson and D. Briggs, *High Resolution XPS of Organic Polymers - The Scienta ESCA300 Database*, Wiley Interscience, 1992, Appendices 3.1 and 3.2.
50 M. C. Biesinger, L. W. M. Lau, A. R. Gerson and R. S. C. Smart, *Appl. Surf. Sci.*, 2010, **257**, 887–898.
51 N. C. Saha and H. G. Tompkins, *J. Appl. Phys.*, 1992, **72**, 3072–3079.
52 M. V. Kuznetsov, J. F. Zhuravlev, V. A. Zhilyaev and V. A. Gubanov, *J. Electron Spectrosc. Relat. Phenom.*, 1992, **58**, 1–9.
53 N. C. Saha and H. G. Tompkins, *J. Appl. Phys.*, 1992, **72**, 3072–3079.
54 CCDC 2447455: Experimental Crystal Struture Determination, 2025, DOI: 10.5517/ccdc.csd.cc2n4s5s.